# LJMU Research Online

Dong, S, Shappee, BJ, Prieto, JL, Jha, SW, Stanek, KZ, Holoien, TW-S, Kochanek, CS, Thompson, TA, Morrell, N, Thompson, IB, Basu, U, Beacom, JF, Bersier, D, Brimacombe, J, Brown, JS, Chen, P, Conseil, E, Danilet, AB, Falco, E, Grupe, D, Kiyota, S, Masi, G, Nicholls, B, Olivares, F, Pignata, G, Pojmanski, G, Simonian, GV, Szczygiel, DM and Wozniak, PR

 ASASSN-15lh: A highly super-luminous supernova

http://researchonline.ljmu.ac.uk/id/eprint/1684/

**Article**

# ASASSN-15lh:
# A Highly Super-Luminous Supernova

Subo Dong,[1*] B. J. Shappee,[2,3] J. L. Prieto,[4,5] S. W. Jha,[6] K. Z. Stanek,[7,8]
T. W.-S. Holoien,[7,8] C. S. Kochanek,[7,8] T. A. Thompson,[7,8] N. Morrell,[9]
I. B. Thompson,[2] U. Basu,[7] J. F. Beacom,[7,8,10] D. Bersier, [11] J. Brimacombe,[12]
J. S. Brown,[7] F. Bufano,[13] Ping Chen,[14] E. Conseil,[15] A. B. Danilet,[7] E. Falco,[16]
D. Grupe,[17] S. Kiyota,[18] G. Masi,[19] B. Nicholls,[20] F. Olivares E.,[21,5] G. Pignata,[21,5]
G. Pojmanski,[22] G. V. Simonian,[7] D. M. Szczygiel,[22] P. R. Woźniak[23]

[1] Kavli Institute for Astronomy and Astrophysics, Peking University, Yi He Yuan Road 5, Hai Dian District, Beijing 100871, China

[2] Carnegie Observatories, 813 Santa Barbara Street, Pasadena, CA 91101, USA

[3] Hubble and Carnegie-Princeton Fellow

[4] Núcleo de Astronomía de la Facultad de Ingeniería, Universidad Diego Portales, Av. Ejército 441, Santiago, Chile

[5] Millennium Institute of Astrophysics, Santiago, Chile

[6] Department of Physics and Astronomy, Rutgers, The State University of New Jersey, 136 Frelinghuysen Road, Piscataway, NJ 08854, USA

[7] Department of Astronomy, The Ohio State University, 140 W. 18th Ave., Columbus, OH 43210, USA

[8] Center for Cosmology and AstroParticle Physics (CCAPP), The Ohio State University, 191 W. Woodruff Ave., Columbus, OH 43210, USA

[9] Las Campanas Observatory, Carnegie Observatories, Casilla 601, La Serena, Chile,

[10] Department of Physics, The Ohio State University, 191 W. Woodruff Ave., Columbus, OH 43210, USA

[11] Astrophysics Research Institute, Liverpool John Moores University, 146 Brownlow Hill, Liverpool L3 5RF, UK

[12] Coral Towers Observatory, Cairns, Queensland 4870, Australia

[13] INAF-Osservatorio Astrofisico di Catania, Via S.Sofia 78, 95123, Catania, Italy

[14] Department of Astronomy, Peking University, Yi He Yuan Road 5, Hai Dian District, 100871, P. R. China

[15] Association Francaise des Observateurs d'Etoiles Variables (AFOEV), Observatoire de Strasbourg 11, rue de l'Universit, F-67000 Strasbourg, France

[16] Harvard-Smithsonian Center for Astrophysics, 60 Garden St., Cambridge, MA 02138, USA.

[17] Department of Earth and Space Science, Morehead State University, 235 Martindale Dr., Morehead, KY 40351, USA

[18] Variable Star Observers League in Japan (VSOLJ), 7-1 Kitahatsutomi, Kamagaya, Chiba 273-0126, Japan

[19] The Virtual Telescope Project, Via Madonna de Loco 47, 03023 Ceccano, Italy

[20] Mt Vernon Observatory, 6 Mt Vernon pl, Nelson, New Zealand

[21] Departamento Ciencias Fisicas, Universidad Andres Bello, Av. Republica 252, Santiago, Chile

[22] Warsaw University Astronomical Observatory, Al. Ujazdowskie 4, 00-478 Warsaw, Poland

[23] Los Alamos National Laboratory, Mail Stop B244, Los Alamos, NM 87545, USA

[*]To whom correspondence should be addressed; E-mail: dongsubo@pku.edu.cn.

**We report the discovery of ASASSN-15lh (SN 2015L), which we interpret as the most luminous supernova yet found. At redshift $z = 0.2326$, ASASSN-15lh reached an absolute magnitude of $M_{u,\mathrm{AB}} = -23.5 \pm 0.1$ and bolometric luminosity $L_{\mathrm{bol}} = (2.2 \pm 0.2) \times 10^{45}$ ergs s$^{-1}$, which is more than twice as luminous as any previously known supernova. It has several major features characteristic of the hydrogen-poor super-luminous supernovae (SLSNe-I), whose energy sources and progenitors are currently poorly understood. In contrast to most previously known SLSNe-I that reside in star-forming dwarf galaxies, ASASSN-15lh appears to be hosted by a luminous galaxy ($M_K \simeq -25.5$) with little star formation. In the 4 months since first detection, ASASSN-15lh radiated $(1.1 \pm 0.2) \times 10^{52}$ ergs, challenging the magnetar model for its engine.**

Only within the past two decades has the most luminous class of supernovae (super-luminous supernovae, SLSNe) been identified (e.g., (*1*)). Compared with the most commonly discovered SNe (Type Ia), SLSNe are more luminous by over two magnitudes at peak and rarer by at least 3 orders of magnitude (*2*). Like normal SNe, SLSNe are classified by their spectra as either SLSN-I (hydrogen-poor) or SLSN-II (hydrogen-rich). Yet the physical characteristics of

2

SLSNe may not be simple extensions from their low-luminosity counterparts (*1*). In particular, the power source for SLSNe-I is poorly understood (*3*). Adding to the puzzle, SLSNe tend to explode in low-luminosity, star-forming dwarf galaxies (*4–6*). The recent advent of wide-area, un-targeted transient surveys has made the systematic discovery and investigation of the SLSNe population possible (e.g., see (*7*) and (*8*) and references therein).

The All-Sky Automated Survey for SuperNovae (ASAS-SN[1]; (*9*)) scans the visible sky every 2–3 nights to depths of $V \simeq 16.5 - 17.3$ mag using a global network of 14 cm telescopes (*9*) in an un-targeted search for new transients, particularly bright supernovae.

On 2015 June 14 [2], ASAS-SN triggered on a new source located at RA $= 22^h 02^m 15\overset{s}{.}45$ Dec $= -61°39'34\overset{''}{.}6$ (J2000), coinciding with a galaxy of then unknown redshift, APMUKS(BJ) B215839.70−615403.9 (*10*). Upon confirmation with our follow-up telescopes, we designated this new source ASASSN-15lh and published its coordinates (*11*).

By combining multiple epochs of ASAS-SN images we extended the detections to fainter fluxes, finding pre-discovery images of ASASSN-15lh from May 8, 2015 ($V = 17.39 \pm 0.23$ mag), and Figure 1 shows the light curve through 2015 September 19. The ASAS-SN light curve peaked at $V = 16.9 \pm 0.1$ on approximately $t_{\mathrm{peak}} \sim$ JD2457179 (June 05, 2015) based on a parabolic fit to the lightcurve (dashed line, Fig. 1). Follow-up images were taken with the Las Cumbres Observatory Global Telescope Network (LCOGT) 1-m telescopes, and the $BV$ light-curves with the galaxy contribution subtracted are also shown.

We obtained an optical spectrum ($3700 - 9200$ Å) of ASASSN-15lh on 2015 June 21 with the du Pont 100-inch telescope. The steep spectral slope with relatively high blue flux motivated *Swift* UVOT/XRT (*12*) target-of-opportunity observations starting on June 24, 2015. The 6-band *Swift* light curve spanning from the UV to the optical ($1928$ Å$-5468$ Å) is shown in Figure 1. The *Swift* spectral energy distribution (SED), peaking in the UV, indicates the source has a high

---

[1]http://www.astronomy.ohio-state.edu/∼assassin/
[2]UT dates are used throughout this paper

temperature. We derive a $3\sigma$ X-ray flux limit of $< 1.6 \times 10^{-14} \,\mathrm{ergs\,s^{-1}\,cm^{-2}}$ (0.3-10 keV) from a total XRT exposure of 81 ks taken between 2015 June 24 and Sep 18.

The du Pont spectrum is mostly featureless (Figure 2, panel (A), first from the top) except for a deep, broad absorption trough near $\sim 5100\,\text{Å}$ (observer frame). SNID ([13]), a commonly used SN classification software that has a spectral library of most types of supernovae except SLSN, failed to find a good SN match. However, we noticed a resemblance between the trough and a feature attributed to O II absorption near $4100\,\text{Å}$ (rest frame) in the spectrum of PTF10cwr/SN2010gx, a SLSN-I at $z = 0.230$ (*3, 14, 15*). Assuming that the ASASSN-15lh absorption trough (FWHM $\sim 10^4 \,\mathrm{km\ s^{-1}}$) was also due to the same feature indicated a similar redshift of $z \sim 0.23$. An optical spectrum $(3250 - 6150\,\text{Å})$ obtained on the Southern African Large Telescope (SALT) revealed a clear Mg II absorption doublet ($\lambda\lambda 2796, 2803$) at $z = 0.232$, confirming the redshift expected from our tentative line identification. Subsequent Magellan/Clay (July 6) and SALT (July 7) spectra refined the redshift to $z = 0.2326$ (panels (C) and (D), Figure 2). The available rest frame spectra show continua with steep spectral slope, relatively high blue fluxes and several broad absorption features also seen in PTF10cwr/SN2010gx (features 'a', 'b' and 'c' labeled in panel (A) of Figure 2) and without hydrogen or helium features, consistent with the main spectral features of SLSNe-I (*1, 3*). The broad absorption feature near $4400\,\text{Å}$ ('d' in Figure 2) seen in PTF10cwr/SN2010gx is not present in ASASSN-15lh. ASASSN-15lh thus has some distinct spectral characteristics in comparison with PTF10cwr/SN2010gx and some other SLSNe-I (*3*).

Using a luminosity distance of $1171\,\mathrm{Mpc}$ (standard *Planck* cosmology at $z = 0.2326$), Galactic extinction of $E(B - V) = 0.03\,\mathrm{mag}$ (*16*), assuming no host extinction (thus the luminosity derived is likely a lower limit), and fitting the *Swift* and LCOGT flux measurements to a simple blackbody (BB) model, we obtain declining rest-frame temperatures of $T_{\mathrm{BB}}$ from $2.1 \times 10^4\,\mathrm{K}$ to $1.3 \times 10^4$ K and bolometric luminosities of $L_{\mathrm{bol}} = 2.2 \times 10^{45}$ to

$0.4 \times 10^{45}\,\mathrm{ergs\ s^{-1}}$ at rest-frame phases relative to the peak of $t_{\mathrm{rest}} \sim 15$ and $\sim 50\,\mathrm{days}$, respectively (see Figure 3). ASASSN-15lh's bolometric magnitude declines at a best-fit linear rate of $0.048\,\mathrm{mag/day}$, which is practically identical to SLSN-I iPTF13ajg (*17*) at $0.049\,\mathrm{mag/day}$ during similar phases ($\sim 10$ to $\sim 50\,\mathrm{days}$). Subsequently, the luminosity and temperature reaches a "plateau" phase with slow changes and a similar trend is also seen for iPTF13ajg though with sparser coverage. Overall, the temperature and luminosity time evolution resemble iPTF13ajg, but ASASSN-15lh has a systematically higher temperature at similar phases. The estimated BB radius of $\sim 5 \times 10^{15}\,\mathrm{cm}$ near the peak is similar to those derived for other SLSNe-I (see, e.g., (*3, 17*)). These similarities in the evolution of key properties support the argument that ASASSN-15lh is a member of the SLSN-I class but with extreme properties.

The absolute magnitudes (AB) in the rest-frame $u$-band are shown in Figure 4. Using either $T_{\mathrm{BB}}$ or the spectra, there is little K-correction (*18*) in converting from $B$-band to rest-frame $u_{\mathrm{AB}}$ with $\mathrm{K}_{B \to u_{\mathrm{AB}}} = -0.1$. The solid red points at $t_{\mathrm{rest}} \gtrsim 10\,\mathrm{days}$ include $B$-band data. Before $\sim 10\,\mathrm{days}$ we lack measurements in blue bands. To estimate $M_{u,\mathrm{AB}}$ at these earlier epochs we assume the $B - V = -0.3\,\mathrm{mag}$ color and K-corrections found for the later epochs with *Swift* photometry. We estimate an integrated bolometric luminosity radiated of $\sim (1.1 \pm 0.2) \times 10^{52}\,\mathrm{ergs}$ over $108\,\mathrm{days}$ in the rest frame. Although our estimates at $t_{\mathrm{rest}} \lesssim 10\,\mathrm{days}$ should be treated with caution, we can securely conclude that the peak $M_{u,\mathrm{AB}}$ is at or brighter than $-23.5 \pm 0.1$, with a bolometric luminosity at or greater than $(2.2 \pm 0.2) \times 10^{45}\,\mathrm{ergs\ s^{-1}}$. Both values are without precedent for any supernova recorded in the literature. In Figure 4, we compare ASASSN-15lh with a sample of SLSNe-I (*3, 17*). Although its spectra resemble the SLSNe-I subclass, ASASSN-15lh stands out from the luminosity distribution of known SLSNe-I, whose luminosities are narrowly distributed around $M \sim -21.7$ (*2, 19*). In Table S1, we list the peak luminosities of the five most luminous SNe discovered to date, including both SLSN-I and SLSN-II. The spectral correspondence and similarities in temperature, luminosity and radius

evolutions between ASASSN-15lh and some SLSNe-I leads to the conclusion that ASASSN-15lh is the most luminous supernova yet discovered. Even though we find that SLSN-I is the most plausible classification of ASASSN-15lh, it is important to consider other interpretations given its distinct properties. We discuss alternative physical interpretations of ASASSN-15lh in the Supplementary text, and given all the currently available data, we conclude that it is most likely a supernova, albeit an extreme one.

The rate of events with similar luminosities to ASASSN-15lh is uncertain. Based on a simple model of transient light curves in ASAS-SN observations tuned to reproduce the magnitude distribution of ASAS-SN Type Ia supernovae (see Supplementary text), the discovery of one ASASSN-15lh-like event implies a rate of $r \simeq 0.6 \, \mathrm{Gpc}^{-3} \, \mathrm{yr}^{-1}$ (90% confidence: $0.21 < r < 2.8$). This is at least 3 times and can be as much as 100 times smaller than the overall rate of SLSNe-I, $r \simeq 32 \, \mathrm{Gpc}^{-3} \, \mathrm{yr}^{-1}$ (90% confidence: $6 < r < 109$) from (*2*), and suggests a steeply falling luminosity function for such supernovae.

For a redshift of $z = 0.2326$, the host galaxy of ASASSN-15lh has $M_K \approx -25.5$, which is much more luminous than the Milky Way. We estimate an effective radius for the galaxy of $2.4 \pm 0.3 \, \mathrm{kpc}$ and a stellar mass of $M_\star \approx 2 \times 10^{11} \, \mathrm{M}_\odot$. This is in contrast to the host galaxies of other SLSNe, which tend to have much lower $M_\star$ (e.g., (*4–6*)). However, given the currently available data, we cannot rule out the possibility that the host is a dwarf satellite galaxy seen in projection. The lack of narrow hydrogen and oxygen emission lines from the galaxy superimposed in the supernova spectra implies little star formation $\mathrm{SFR} < 0.3 \, \mathrm{M}_\odot$ $\mathrm{yr}^{-1}$ by applying the conversions in (*20*). LCOGT astrometry places ASASSN-15lh within $0.''2$ (750 pc) of the center of the nominal host. A detailed discussion of the host properties is provided in the supplementary text.

The power source for ASASSN-15lh is unknown. Traditional mechanisms invoked for normal SNe likely cannot explain SLSNe-I (*3*). The lack of hydrogen or helium suggests that shock

interactions with hydrogen-rich circumstellar material, invoked to interpret some SLSNe, cannot explain SLSNe-I or ASASSN-15lh. SLSN-I post-peak decline rates appear too fast to be explained by the radioactive decay of $^{56}$Ni (3) – the energy source for Type Ia supernovae. Both the decline rate of the late-time light curve and the integral method (21) will allow tests of whether ASASSN-15lh is powered by $^{56}$Ni, and we estimate that $\gtrsim 30\,M_\odot$ of $^{56}$Ni would be required to produce ASASSN-15lh's peak luminosity. Another possibility is that the spindown of a rapidly-rotating, highly-magnetic neutron star (a magnetar) powers the extraordinary emission (22–24). To match the peak $L_{\mathrm{bol}}$ and timescale of ASASSN-15lh, the light-curve models of (23) imply a magnetar spin period and magnetic field strength of $P \simeq 1\,\mathrm{ms}$ and $B \simeq 10^{14}\,\mathrm{G}$, respectively, assuming that all of the spindown power is thermalized in the stellar envelope. If efficient thermalization continues, this model predicts an $L_{\mathrm{bol}} \propto t^{-2}$ power-law at late times. The total observed energy radiated so far ($1.1 \pm 0.2 \times 10^{52}$ ergs) strains a magnetar interpretation because, for $P \lesssim 1\,\mathrm{ms}$, gravitational wave radiation should limit the total rotational energy available to $E_{\mathrm{rot}}^{\mathrm{max}} \sim 3 \times 10^{52}$ ergs (25) and the total radiated energy to a third of $E_{\mathrm{rot}}^{\mathrm{max}}$, which is $\sim 10^{52}$ ergs (23).

The extreme luminosity of ASASSN-15lh opens up the possibility of observing such supernovae in the early universe. An event similar to ASASSN-15lh could be observed with the Hubble Space Telescope out to $z \sim 6$, and with the James Webb Space Telescope out to $z \gtrsim 10$ (19). A well-observed local counterpart will be critical in making sense of future observations of the transient high-redshift universe.

# References and Notes

1. A. Gal-Yam, *Science* **337**, 927 (2012).

2. R. M. Quimby, F. Yuan, C. Akerlof, J. C. Wheeler, *Mon. Not. R. Astron. Soc.* **431**, 912

(2013).

3. R. M. Quimby, *et al.*, *Nature* **474**, 487 (2011).

4. J. D. Neill, *et al.*, *Astrophys. J.* **727**, 15 (2011).

5. R. Stoll, *et al.*, *Astrophys. J.* **730**, 34 (2011).

6. R. Lunnan, *et al.*, *Astrophys. J.* **787**, 138 (2014).

7. R. M. Quimby, *IAU Symposium*, A. Ray, R. A. McCray, eds. (2014), vol. 296 of *IAU Symposium*, pp. 68–76.

8. M. Nicholl, *et al.*, *Mon. Not. R. Astron. Soc.* **452**, 3869 (2015).

9. B. J. Shappee, *et al.*, *Astrophys. J.* **788**, 48 (2014).

10. S. J. Maddox, G. Efstathiou, W. J. Sutherland, J. Loveday, *Mon. Not. R. Astron. Soc.* **243**, 692 (1990).

11. B. Nicholls, *et al.*, *The Astronomer's Telegram* **7642**, 1 (2015).

12. D. N. Burrows, *et al.*, *Space Sci. Rev.* **120**, 165 (2005).

13. S. Blondin, J. L. Tonry, *Astrophys. J.* **666**, 1024 (2007).

14. A. Pastorello, *et al.*, *Astrophys. J. L.* **724**, L16 (2010).

15. C. Inserra, *et al.*, *Astrophys. J.* **770**, 128 (2013).

16. E. F. Schlafly, D. P. Finkbeiner, *Astrophys. J.* **737**, 103 (2011).

17. P. M. Vreeswijk, *et al.*, *Astrophys. J.* **797**, 24 (2014).

18. D. W. Hogg, I. K. Baldry, M. R. Blanton, D. J. Eisenstein, *ArXiv Astrophysics e-prints:astro-ph/0210394* (2002).

19. C. Inserra, S. J. Smartt, *Astrophys. J.* **796**, 87 (2014).

20. S. Savaglio, K. Glazebrook, D. Le Borgne, *Astrophys. J.* **691**, 182 (2009).

21. B. Katz, D. Kushnir, S. Dong, *ArXiv e-prints, arXiv:1301.6766* (2013).

22. P. Bodenheimer, J. P. Ostriker, *Astrophys. J.* **191**, 465 (1974).

23. D. Kasen, L. Bildsten, *Astrophys. J.* **717**, 245 (2010).

24. S. E. Woosley, *Astrophys. J. Lett.* **719**, L204 (2010).

25. B. D. Metzger, D. Giannios, T. A. Thompson, N. Bucciantini, E. Quataert, *Mon. Not. R. Astron. Soc.* **413**, 2031 (2011).

26. O. Yaron, A. Gal-Yam, *Pub. Astron. Soc. Pac.* **124**, 668 (2012).

27. C. Alard, *Astron. Astrophys.* **144**, 363 (2000).

28. T. S. Poole, *et al.*, *Mon. Not. R. Astron. Soc.* **383**, 627 (2008).

29. A. A. Breeveld, *et al.*, *Mon. Not. R. Astron. Soc.* **406**, 1687 (2010).

30. P. J. Brown, *The Astronomer's Telegram* **8086**, 1 (2015).

31. R. Margutti, *The Astronomer's Telegram* **8089**, 1 (2015).

32. D. Lang, D. W. Hogg, K. Mierle, M. Blanton, S. Roweis, *Astronomical Journal* **139**, 1782 (2010).

33. A. A. Henden, S. Levine, D. Terrell, D. L. Welch, *American Astronomical Society Meeting Abstracts* (2015), vol. 225 of *American Astronomical Society Meeting Abstracts*, p. 336.16.

34. S. M. Crawford, *et al.*, *Society of Photo-Optical Instrumentation Engineers (SPIE) Conference Series* (2010), vol. 7737 of *Society of Photo-Optical Instrumentation Engineers (SPIE) Conference Series*, p. 25.

35. A. J. Drake, *et al.*, *Astrophys. J.* **696**, 870 (2009).

36. R. G. McMahon, *et al.*, *The Messenger* **154**, 35 (2013).

37. E. Bertin, S. Arnouts, *Astronomy and Astrophysics, Supplement* **117**, 393 (1996).

38. P. Melchior, A. Drlica-Wagner, K. Bechtol, E. Rykoff, W. H. D. E. Survey, *The Astronomer's Telegram* **7843**, 1 (2015).

39. M. Kriek, *et al.*, *Astrophys. J.* **700**, 221 (2009).

40. G. Bruzual, S. Charlot, *Mon. Not. R. Astron. Soc.* **344**, 1000 (2003).

41. C. Y. Peng, L. C. Ho, C. D. Impey, H.-W. Rix, *Astronomical Journal* **124**, 266 (2002).

42. T.-W. Chen, *et al.*, *The Astrophysical Journal Letters* **763**, L28 (2013).

43. R. Lunnan, *et al.*, *Astrophys. J.* **804**, 90 (2015).

44. T.-W. Chen, *et al.*, *Mon. Not. R. Astron. Soc.* **452**, 1567 (2015).

45. R. M. Quimby, *et al.*, *The Astronomer's Telegram* **4121**, 1 (2012).

46. V. Stanishev, *et al.*, *Astron. Astrophys.* **469**, 645 (2007).

47. A. Clocchiatti, N. B. Suntzeff, R. Covarrubias, P. Candia, *Astronomical Journal* **141**, 163 (2011).

48. M. C. Bersten, M. Hamuy, *Astrophys. J.* **701**, 200 (2009).

49. N. B. Suntzeff, P. Bouchet, *Astronomical Journal* **99**, 650 (1990).

50. T. C. Licquia, J. A. Newman, J. Brinchmann, *Astrophys. J.* **809**, 96 (2015).

51. C. S. Kochanek, *Saas-Fee Advanced Course 33: Gravitational Lensing: Strong, Weak and Micro*, G. Meylan, *et al.*, eds. (2006), pp. 91–268.

52. C. L. MacLeod, *et al.*, *Astrophys. J.* **721**, 1014 (2010).

53. D. E. Vanden Berk, *et al.*, *Astrophys. J.* **601**, 692 (2004).

54. B. M. Peterson, *An Introduction to Active Galactic Nuclei* (1997).

55. A. J. Drake, *et al.*, *Astrophys. J.* **735**, 106 (2011).

56. I. Arcavi, *et al.*, *Astrophys. J.* **793**, 38 (2014).

57. S. Gezari, *et al.*, *Nature* **485**, 217 (2012).

58. L. E. Strubbe, N. Murray, *ArXiv e-prints:1509.04277* (2015).

59. T. W.-S. Holoien, *et al.*, *Mon. Not. R. Astron. Soc.* **445**, 3263 (2014).

60. T. W.-S. Holoien, *et al.*, *ArXiv e-prints:1507.01598* (2015).

61. J. Vinkó, *et al.*, *Astrophys. J.* **798**, 12 (2015).

62. R. Chornock, *et al.*, *Astrophys. J.* **780**, 44 (2014).

63. N. Häring, H.-W. Rix, *Astrophys. J. Lett.* **604**, L89 (2004).

64. S. Benetti, *et al.*, *Mon. Not. R. Astron. Soc.* **441**, 289 (2014).

65. A. A. Miller, *et al.*, *Astrophys. J.* **690**, 1303 (2009).

# Acknowledgement

**Figure 1. Multi-band light curve of ASASSN-15lh.** The *V*-band ASAS-SN light curve is shown as black solid dots, and upper limits are represented by black arrows. *Swift* and LCOGT 1-m data are shown as open circles.

13
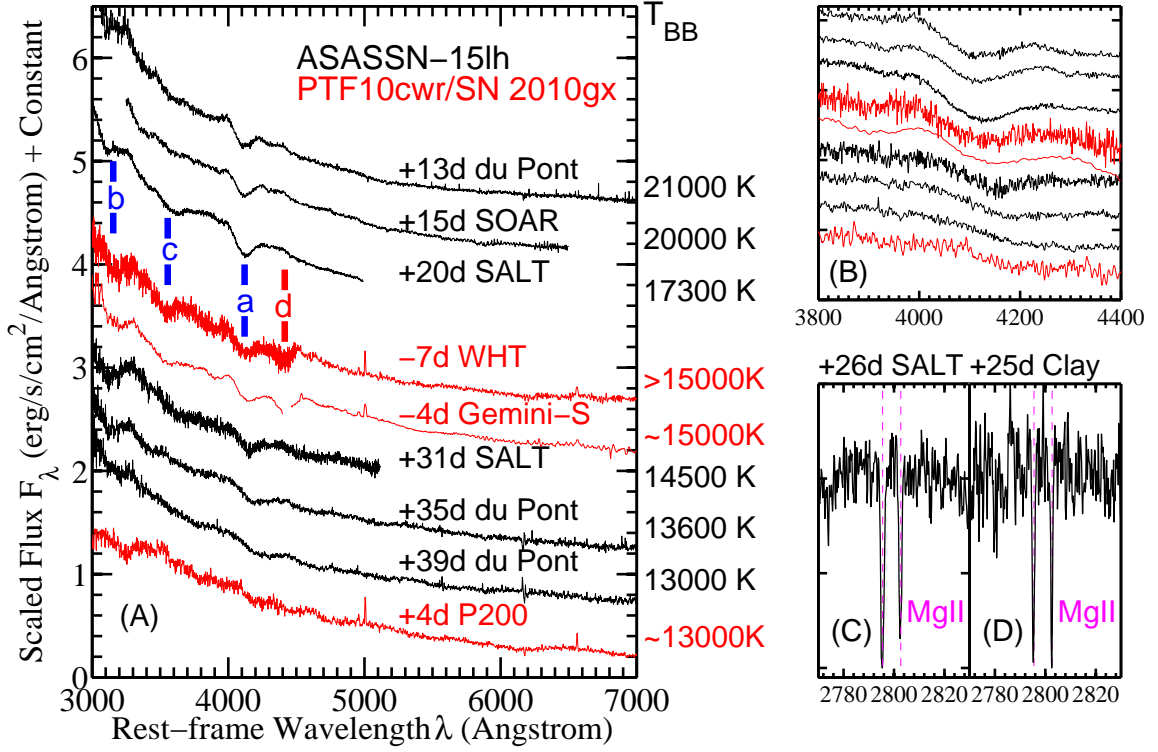
**Figure 2. Rest-frame spectra of ASASSN-15lh (black) compared with SLSN-I PTF10cwr/SN 2010gx (red).** (A): The spectra are offset for clarity, labelled with phases and telescopes, and they are ranked by descending $T_{BB}$ (given on the right) from the top. The ASASSN-15lh spectra are blue and featureless, except for broad absorption features labelled 'a', 'b' and 'c' (marked in blue), which match those of PTF10cwr/SN 2010gx at similar $T_{BB}$. Absorption features 'a' at $\sim 4100\,\text{Å}$ and 'd' at $\sim 4400\,\text{Å}$ (marked in red) in PTF10cwr/SN 2010gx are commonly attributed to O II (e.g., (*3, 15*)). The $\sim 4400\,\text{Å}$ feature is not present in ASASSN-15lh. Panel (B) shows close-ups of the $4100\,\text{Å}$ features, whose evolution in shape, depth and velocity as a function of $T_{BB}$ is similar for both supernovae. The ASASSN-15lh host redshift ($z = 0.2326$) is determined from the Mg II doublets seen in the SALT and Clay MagE spectra (panels (C) and (D)), with EW $0.55 \pm 0.05\text{Å}$ and $0.49 \pm 0.05\text{Å}$, respectively.

14
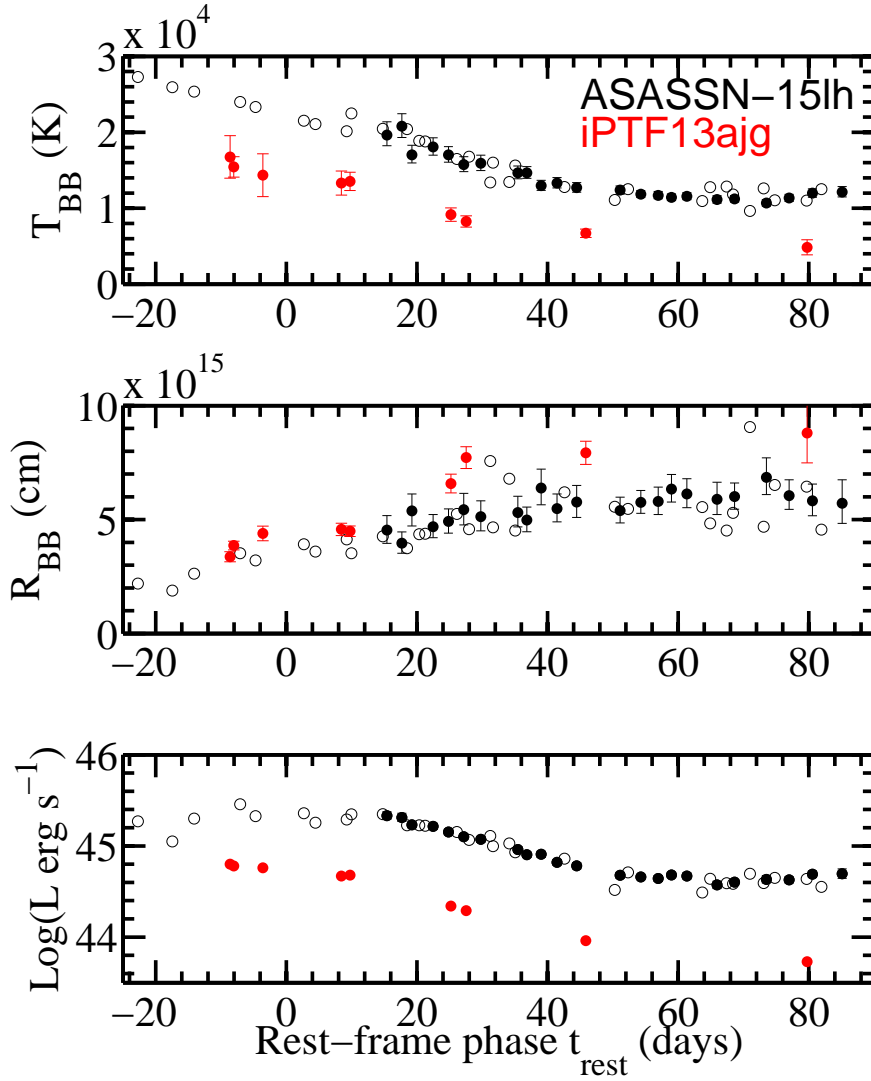
**Figure 3. Time evolution of blackbody temperatures, radii and bolometric luminosities for ASASSN-15lh (black) and SLSN-I iPTF13ajg (red).** Solid black dots show estimates derived from the full UV and optical bands whereas the open circles show those from optical only. For $t_{\rm rest} < 10\,{\rm days}$, only V-band is availablFe and the temperatures are estimated based on linear extrapolation from MJD$= 57191 - 57241$.
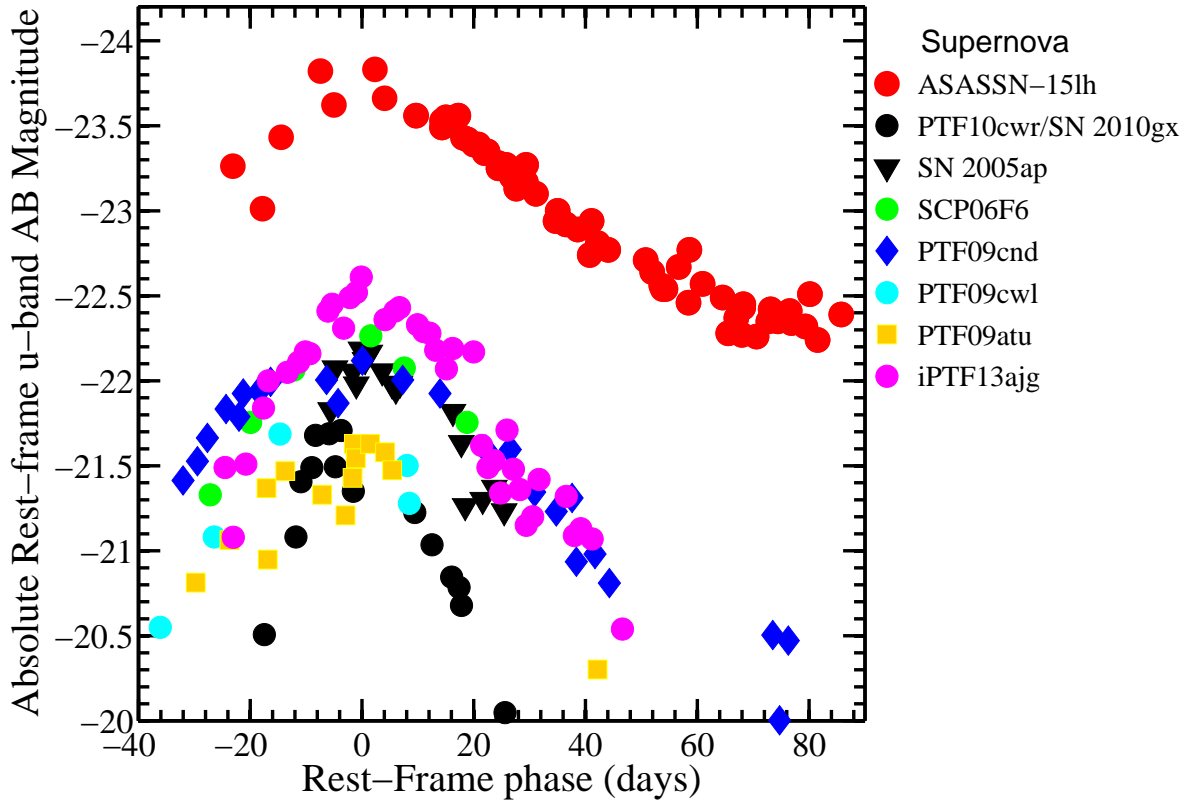
**Figure 4. Rest-frame absolute magnitude light curve of ASASSN-15lh near peak compared with other SLSNe-I.** Estimates of $M_{u,\mathrm{AB}}$ for ASASSN-15lh at $t_{\mathrm{rest}} \gtrsim 10\,\mathrm{days}$ are derived from $B$-band fluxes, which are subject to small K-corrections, whereas the less reliable $M_{u,\mathrm{AB}}$ estimates are based on $V$-band only for $t_{\mathrm{rest}} \lesssim 10\,\mathrm{days}$. The comparison sample (*3, 17*) includes the most luminous SLSNe-I previously known. At $M_{u,\mathrm{AB}} = -23.5$, ASASSN-15lh stands out from the SLSNe-I luminosity distribution (*2, 19*). Its peak bolometric absolute magnitude is more than $\sim 1\,\mathrm{mag}$ more luminous than any other SLSN-I.

# Supplementary Materials for

## ASASSN-15lh: A Highly Super-Luminous Supernova

Subo Dong,[1][*] B. J. Shappee,[2,3] J. L. Prieto,[4,5] S. W. Jha,[6] K. Z. Stanek,[7,8]

T. W.-S. Holoien,[7,8] C. S. Kochanek,[7,8] T. A. Thompson,[7,8] N. Morrell,[9]

I. B. Thompson,[2] U. Basu,[7] J. F. Beacom,[7,8,10] D. Bersier, [11] J. Brimacombe,[12]

J. S. Brown,[7] F. Bufano,[13] Ping Chen,[14] E. Conseil,[15] A. B. Danilet,[7] E. Falco,[16]

D. Grupe,[17] S. Kiyota,[18] G. Masi,[19] B. Nicholls,[20] F. Olivares E.,[21,5] G. Pignata,[21,5]

G. Pojmanski,[22] G. V. Simonian,[7] D. M. Szczygiel,[22] P. R. Woźniak[23]

Correspondence to: dongsubo@pku.edu.cn.

**This PDF file includes:**

# 1    Data Acquisitions & Reductions

The ASAS-SN images were processed by the fully automatic ASAS-SN pipeline (Shappee et al. in prep.) which uses the ISIS image subtraction package (*27*). Upon careful examination, we marginally detected ASASSN-15lh in a number of pre-discovery images from two cameras (5 and 6) on the ASAS-SN southern unit, Cassius. Fig. S1 presents the reference images for both cameras constructed from data obtained between May and December 2014. These reference images allow us to remove any host-galaxy light. To recover a more robust light curve of the event, we combined individual 90-second subtracted images that were taken within 7.5 days of each other and acquired on the same camera (averaging $2 - 8$ images). We find that ASASSN-15lh was first detected in a stack of 6 images acquired between May 4-11, 2015 ($V \sim 17.4$ mag). The derived Johnson $V$ magnitudes are reported in Table S4. In Fig. S1 we show an example from before and after peak, one from each camera, demonstrating the quality of our subtractions and detections of ASASSN-15lh.

Following the discovery of the transient, we obtained a series of 32 *Swift* XRT and UVOT target-of-opportunity (ToO) observations between 2015 June 24 and 2015 September 19. The UVOT observations were obtained in 6 filters: $V$ (5468 Å), $B$ (4392 Å), $U$ (3465 Å), $UVW1$ (2600 Å), $UVM2$ (2246 Å), and $UVW2$ (1928 Å) (*28*). We used a $5.''0$ radius region to extract source counts and a $\sim 40.''0$ radius region to extract background counts via the software task UVOTSOURCE. We then used the UVOT calibrations from (*28*) and (*29*) to convert the measured count rates into magnitudes and fluxes. The magnitudes are reported in the Vega system in Table S5. We analyzed all available X-ray data obtained by the Swift XRT until 2015 September 18. In this 81 ks exposure we found a 3 sigma upper limit at a level of $3.2 \times 10^{-4}$ counts s$^{-1}$ in the Swift XRT. Using a standard power-law spectrum with a 0.3-10 keV spectral slope $\alpha_X = 1.0$ and galactic absorption, this upper limit converts to $1.6 \times 10^{-14}$ ergs s$^{-1}$ cm$^{-2}$. The SWIFT multi-

band photometry plays an important in deriving the bolometric luminosity and SED evolutions. Three months since the first SWIFT observations, the SWIFT colors have evolved redder and UV fluxes have dropped by $\sim 2\,\mathrm{mag}$. Since phase $t_{\mathrm{test}} \sim 50\,\mathrm{days}$, the fluxes from optical and UV have kept approximately constant, entering into a plateau phase with an increase in UV fluxes near $\sim 80\,\mathrm{days}$ (see also (*30, 31*)).

We retrieved the reduced (bias subtracted and flat-fielded) LCOGT $BV$ images from the LCOGT image archive. We solved for the astrometry of the images using astrometry.net (*32*) and ran PSF fitting photometry with DoPHOT to extract the photometry of ASASSN-15lh. The magnitude zero points were obtained from photometry of stars in the field from the AAVSO Photometric All-Sky Survey (APASS; (*33*)). The magnitudes are reported in Table S6.

Note that in order to derive the fluxes of the supernova, we subtract the host galaxy fluxes (derived in the following section) from the SWIFT and LCOGT for $B$ and $V$ bands. As can be seen from the host SED discussed in the section below, the host is red and thus its fluxes in bands bluer than $B$ are negligible as compared to those of the supernova at the epochs of interest.

The single-slit spectra from the Wide Field Reimaging CCD Camera (WFCCD) on 2015 June 21 on the du Pont 100-inch Telescope and the Goodman Spectrograph on the Southern Astrophysical Research Telescope (SOAR) were obtained at the parallactic angle and reduced with standard routines in the IRAF `twodspec` and `onedspec` packages. The reductions included bias subtraction, flat-fielding, 1-D spectral extraction, wavelength calibration using an arc lamp, and flux calibration using a spectroscopic standard usually taken the same night.

The Southern African Large Telescope (SALT) observations were obtained with the Robert Stobie Spectrograph (RSS), using an atmospheric dispersion corrector and $1\rlap{.}{''}5$ longslit oriented at a position angle of $127.7°$ east of north to include a bright reference star on the slit. The spectrum taken on UT 2015-Jun-30.17 had 2100 sec of total exposure with the PG0900 grating

in two tilt positions to fill chip gaps and cover the wavelength range 3250-6150 Å  at a spectral resolution $R = \lambda/\Delta\lambda \approx 900$.  The UT 2015-07-06.99 spectrum used the PG3000 grating in two tilt positions, covering the wavelength range 3340-4080 Å  with a total exposure of 2400 sec and spectral resolution $R \approx 2600$.  These data were reduced with a custom pipeline that incorporates routines from PyRAF and PySALT (*34*).

We calibrate all spectra by extracting synthetic photometric magnitudes for each filter in the spectral range and then finding the best linear fit to the observed magnitudes interpolated to the spectral epoch. For spectra where only a single filter fit within the spectral range, the spectrum was scaled by a constant. The calibrated spectra are shown in Fig. 2 and the digital versions are made available in the public WISeREP (*26*) repository.

## 2   Host Galaxy Properties

We searched public data archives and surveys in order to characterize the candidate host galaxy of ASASSN-15lh, APMUKS(BJ) B215839.70−615403.9 (*10*).  The host is detected in CRTS (*35*) images and the long term $V$-band light curve does not show any strong evidence for photometric variability, with a $V$-band rms of 0.27 mag determined by the photometric uncertainties (see Fig. S2). We found excellent near-infrared $H$ and $K_s$-band images of the host in the European Southern Observatories (ESO) archive from the VISTA Hemisphere Survey (VHS; (*36*)). After calibrating the images using 2MASS stars in the field, we used Sextractor (*37*) to measure total aperture magnitudes of the host of $J = 16.04 \pm 0.03$ mag and $K_s = 14.82 \pm 0.04$ mag, which correspond to absolute magnitudes of $M_J \simeq -24.3$ and $M_{K,s} \simeq -25.5$ for the assumed distance modulus.

To analyze the SED of the host galaxy, we combined the near-IR fluxes that we derived from the VHS images with the $griz$ magnitudes of the host reported from the Dark Energy Survey (DES) data by (*38*). The SED of APMUKS(BJ) B215839.70-615403.9 is shown in Fig. S3.

We also show a fit using stellar population synthesis (SPS) models. The fit was obtained using the Fitting and Assessment of Synthetic Templates (FAST; (*39*)) code using Bruzual & Charlot (2003) SPS models (*40*), assuming a Salpeter IMF and an exponentially declining star-formation history (SFR(t) $\propto$ e$^{-t/\tau}$), and correcting the fluxes for Galactic extinction only. The best SPS model fit from FAST is excellent, with a reduced $\chi^2$ of 0.94, giving a total stellar mass of $\log(M_\star/M_\odot) = 11.34 \pm 0.1$ ($M_\star \simeq 2 \times 10^{11}$ $M_\odot$), $\log(\tau/\text{years}) = 9.10^{+0.20}_{-0.08}$, and $\log(\text{age/years}) = 9.90^{+0.10}_{-0.04}$. Given the good SPS fit of the SED, we used this model to derive synthetic magnitudes in all the Swift/UVOT and LCOGT filters in which we obtained photometry of ASASSN-15lh, in order to use these fluxes for host-galaxy subtraction. The resulting synthetic magnitudes of the host are: $V = 18.92$, $B = 20.47$, $U = 20.69$, $UW1 = 21.13$, $UM2 = 21.18$, and $UW2 = 21.12$ (Swift/UVOT filters in Vega system), $B = 20.37$, $V = 18.89$ (Johnson-Kron/Cousins filters in Vega system).

We also analyzed the archival near-IR images of the host with GALFIT (*41*) in order to fit the morphological structure of the host galaxy in the 2D images. We find excellent (reduced $\chi^2$ of ~1) Sersic profile fits ($\Sigma(r) \propto r^{-n}$) for the $J$ and $K_s$ bands, without the need of extra components (e.g., a disk). The results of the fits are: $n = 3.41 \pm 0.47$ and $R_e = 0\overset{\prime\prime}{.}68 \pm 0\overset{\prime\prime}{.}03$ in the $J$ band image, $n = 4.82 \pm 1.16$ and $R_e = 0\overset{\prime\prime}{.}59 \pm 0.07$ in $K_s$ band image. From these results, the structure of the host galaxy is consistent with a de Vaucouleurs spheroidal profile ($n = 4$), with an effective radius of $2.4 \pm 0.3$ kpc.

The high stellar mass, red colors, spheroidal morphology, and low recent star-formation (obtained from upper limit on [O II] emission lines in the supernova spectra) of APMUKS(BJ) B215839.70-615403.9 make it consistent with an old, massive galaxy. This is in line with the results of (*38*), who found that the SED of the host was that of a red-sequence galaxy at a photometric redshift of $0.25 \pm 0.02$, consistent with the spectroscopic redshift measured from the Mg II doublet in the supernova spectra. The high stellar mass and low star-formation rate

make the candidate host of ASASSN-15lh distinct among SLSN-I host galaxies, which tend to be low-metallicity, low-mass, and high star-formation rate density galaxies (e.g., (*4–6, 42–44*). We note that we cannot rule out the presence of a small dwarf galaxy in projection along the line of sight to this massive, compact galaxy with the current images that we have of the event. Higher resolution data (e.g., with HST) obtained after the supernova fades will be important for fully characterizing the host galaxy.

We perform relative astrometry between the LCOGT (June 16, 2015, $0.''47$/pixel, FWHM = 2.3 pixel) and archival DSS image (July 7, 1995, $1.''01$/pixel, FWHM = 5.0 pixel). Using 10 common bright and isolated stars in the LCOGT field, we establish a 6-parameter coordinate transformation between the images with IRAF `geomap` package. The result of the transformation yields a separation in east (RA) direction of $0.''10 \pm 0.''13$, and north (Decl.) direction $0.''15 \pm 0.''10$ between the transformed LCOGT supernova position and the DSS galaxy centroid position. The supernova was at $V \sim 17$ while the host galaxy has $V \sim 18.9$ so the astrometric separation between the supernova and galaxy centroid is $0.''18 \pm 0.''16$.

# 3  Blackbody Fits and Total Radiated Energy

We fit each epoch with photometric data using a simple blackbody model. For the epochs with Swift data we used no priors on the blackbody temperature $T_{BB}$. From these results we designed a simple logarithmic prior for the epochs with only optical data. The priors were set to be $20000$ K on JD 2457191 and $11000$ K on JD 2457241, varying linear between these dates and constant afterwards. We then considered two models for the earlier phases where either the temperature continued to rise linearly towards earlier times (Table S2) or was held constant for the earlier epochs (Table S3). The temperature prior was applied to $\log_{10} T_{BB}$ with an uncertainty of $0.05$ dex. Parameter uncertainties were determined using Monte Carlo Markov Chain methods. The Tables S2 and S3 report the estimated median luminosities, temperatures,

6

and blackbody radii along with their estimated symmetric 90% confidence regions. The total radiated energy $E$ was determined by trapezoidal integration of the results for the individual epochs. The uncertainties are dominated by the choice of the temperature priors, where a shift of $\pm 2000$ K in the absolute level changes the estimate by $10\%$, and the shift from the constant temperature prior to the rising temperature prior for early times increases the estimate by $10\%$. The span of these systematic uncertainties leads to our estimate that $E = (1.1 \pm 0.2) \times 10^{52}$ erg.

In Fig. S4., we show ASASSN-15lh SEDs (filled circles with error bars) at various phases and respective best-fit blackbody models (lines). The blackbody models are reasonable descriptions of the SEDs with a well-detected UV peak in the SED that is inconsistent with a power-law spectrum.

In Fig. S5, we compare the derived the bolometric light curves of ASASSN-15lh with those of several supernovae of various types. The comparison supernovae include hydrogen-poor SLSN iPTF13ajg (*17*), PTF12dam (*44, 45*), Type Ia supernova SN 2003du (*46*), broad-line Type Ic (Ic-GRB) supernova ("hypernova") SN 1998bw (*47*), Type IIP supernova SN 1999em (*48*) and Type II supernova SN 1987A (*49*). Note that the peak bolometric luminosity of ASASSN-15lh is brighter than that of the Milky Way (*50*) by more than one order of magnitude.

# 4  Rate

While ASASSN-15lh is a single event, we can use it to estimate the rate of such high luminosity SLSNe for comparison to the rate at lower luminosity found by (*2*). We estimate it by randomly drawing light curves for the centers of randomly selected $0.01 < z < 0.1$ SDSS galaxies observed by the ASAS-SN survey for the period 1 June 2014 to 31 May 2015. The goal here is to roughly sample the high latitude sky (e.g. Galactic extinction) and typical weather modulated cadences. Using $0.01 < z < 0.1$ galaxy centers is mildly conservative in that the noise contribution from the galaxies will be mildly overestimated. In general, however, since the vast

majority of these galaxies are undetected in ASAS-SN, the use of these galaxies differs little from using random positions. The primary purpose of the procedure is to supply a random set of observing cadences and their associated noise levels. Although we survey regions closer to the Galactic plane, we assume the sky coverage excludes latitudes $|b| < 10°$.

To estimate the rates, we randomly select a light curve, a redshift assuming a constant comoving density in volume $V_{com}$ and the time at which the transient peaks. The scrambling of the true SDSS redshifts is unimportant. The observed comoving rate and transient time scale are corrected for time dilation. Relative to the time at which they peak, we assume the transients can be modeled as

$$M_V(t) = M_{peak} + (t/t_{peak}(1+z))^2 - 1.86z \tag{1}$$

where $t_{peak}$ is the rest frame time for the light curve to decay by one magnitude and the last term is a simple K-correction matching our estimate for ASASSN-15lh at its observed redshift. For ASASSN-15lh, $t_{peak} \simeq 30$ to $40$ days. Comparing the model fluxes and observed noise at the epochs of the randomly selected light curve, we define a detection as an event where the signal-to-noise ratio is $S/N > 7.5$ for at least two epochs separated by less than one week. This criterion reproduces the observed magnitude distribution of ASAS-SN Type Ia SNe well. From these statistics we obtain the average number of days over which we would detect the model transient for galaxies randomly distributed out to the distance limit, $\langle t \rangle$, leading to a rate estimate for $N$ events of $r = N(\langle t \rangle V_{com})^{-1}$. We tabulated the results for $M_{peak} = -20, -21, -22, -23$ and $-24$ and $t_{peak} = 10, 20, 30$ and $40$ days.

For one detected event, the differential rates for $t_{peak} = 40$ days scale with absolute luminosity as $r = 60, 15, 3.8, 0.96$ and $0.23$ Gpc$^{-3}$ year$^{-1}$ in order of increasing luminosity. Because of ASAS-SN's relatively high cadence, the choice of $t_{peak}$ is unimportant given the statistical uncertainties provided $t_{peak} \geq 20$ days (using $t_{peak} = 30, 20$ or $10$ days instead of $40$ days raises the rate estimates by approximately 3%, 26% and 83%, respectively). Thus,

if we consider ASASSN-15lh as one event over the magnitude range $-23 < M_{peak} < -24$, the mean rate is $r \simeq 0.60$ Gpc$^{-3}$ year$^{-1}$ with $0.21 < r < 2.8$ at 90% confidence given the Poisson uncertainties for one event. The lack of events in the magnitude ranges $-21 < M_{peak} < -22$ and $-22 < M_{peak} < -23$ imply 90% confidence upper limits on the rates of $r < 22$ and $< 5.5$ Gpc$^{-3}$ year$^{-1}$, respectively. This is broadly consistent with (2), who found $r \simeq 32$ Gpc$^{-3}$ year$^{-1}$ ($6 < r < 109$) for SLSNe-I concentrated in the (unfiltered) magnitude range $M_{peak} \simeq -21.7 \pm 0.4$ mag, and the lack of any more luminous examples in (2) is consistent with our inference of a steeply falling luminosity function. Alternately, for the rate found by (2) we would have expected $1.4$ (0.3 to 4.9) events with $-21 < M_{\mathrm{peak}} < -22$, and our failure to find one is compatible with Poisson expectations except at the upper end of their rate estimates. More work is required to fully understand the SLSNe luminosity function and to more completely quantify the ASAS-SN survey efficiency and completeness.

# 5 Alternative Scenarios

In this section, we examine alternative interpretations of ASASSN-15lh other than a superluminous supernova.

At this low redshift, any significant contribution from gravitational lensing is completely implausible (see, e.g., the review by Kochanek 2006 (51) of lens properties and statistics). Moreover, the putative lens (Mg II absorption) and source (broad absorption trough) redshifts are identical.

That the transient's position is consistent with the center of the host galaxy raises the possibility that it is some form of transient created by a supermassive black hole. Of the various possibilities, a plausible scenario is that the transient is a tidal disruption event (TDE) where the debris from tidally destroying a star is then accreted. Normal Active Galactic Nucleus (AGN) activity has been well-characterized as a stochastic process with well-defined properties

(e.g., (52)) that are inconsistent with the observed variability and the spectral slope of the variable flux is not thermal (e.g., (53)). Only blazars and related "jetted" sources show this level of variability, but they also have featureless, non-thermal, power law spectra (see, e.g., (54)). The archival CRTS data (Fig. S2) show no variability at the level of $\sim 0.3 \, \mathrm{mag}$ and is thus consistent with no past AGN activities. We cannot rule out the possibility that the host galaxy has a weak AGN with a level of photometric variability below the CRTS detection limits or the existence of weak AGN emission lines that are below our current spectroscopic detection limits. This issue will likely be clarified by further studying the host as ASASSN-15lh fades.

Nuclear outbursts do occur, with the best example being CSS100217 (55), a nuclear transient in an already active Seyfert galaxy. Its nature is debated (SLSN-II or TDE), but it has prominent and changing hydrogen Balmer lines during the transient, which are not seen at all in ASASSN-15lh spectra, suggesting that they have different origins.

A fundamental problem for interpreting ASASSN-15lh as a TDE is the lack of both hydrogen and helium emission lines. Almost all known TDEs show varying combinations of strong, broad H$\alpha$/H$\beta$ and HeII 4686Å emission lines (e.g. (56)). In the initial phases, the apparent temperature of ASASSN-15lh combined with its luminosity implies the generation of large numbers of ionizing photons ($Q \sim 10^{55}$ s$^{-1}$ above 13.6 eV). A large fraction of these photons photo-ionize hydrogen and helium and must eventually produce recombination lines. The nature of the TDE process makes it very difficult to avoid having moderate density gas associated with the disruption that will do the reprocessing. The balance between hydrogen and helium can vary both due to the composition of the star (e.g., the helium star hypothesis for PS1-10jh, (57)) and variations in the effective temperature. For example, (58) make very strong arguments that the only way to avoid having hydrogen emission lines from PS1-10jh is to have no hydrogen to begin with. By extension, the only way to avoid having both hydrogen and helium emission lines from a TDE is to have neither element, through the disruption of a Wolf-Rayet star stripped of

10

both elements. We also note that the UV/optical spectral energy distributions of TDEs generally are very slowly evolving and hot (staying $\sim 20000$ to $40000$ K for many months after the peak, see (*56, 59, 60*)). Their apparent photospheres do not show the steady cooling and expanding ejecta from explosive events like supernovae or ASASSN-15lh (see Fig. 3).

The event called "Dougie" (*61*) was an off-nuclear transient with a featureless spectra. The temperature evolution from $\sim 13000$ k to $\sim 6300$ K is typical of supernova and not observed in other TDE candidates, both suggesting it was likely a supernova. PS1-11af (*62*) is regarded as a TDE candidate and showed a blue featureless spectra. Its temperature stayed approximately constant for three months after the peak, which is typical for a TDE but significantly differs from ASASSN-15lh. For both "Dougie" and PS1-11af, there are no clear spectral features that resemble those seen in ASASSN-15lh.

Finally, the very massive, compact, and old host of ASASSN-15lh would likely imply a large central supermassive black hole mass (*63*). Since TDEs strongly favor relatively low-mass supermassive black holes, this adds to the argument against the TDE interpretation of ASASSN-15lh.

## Further Acknowledgement

**Figure S1.** Comparisons between the ASAS-SN reference image from camera 5 (top-left), 6 (top-middle), the ASAS-SN stacked subtraction image from camera 5 (bottom-left), 6 (bottom-middle) post-maximum, the archival DECam false-color image ( (*38*);top-right), and stacked false-color follow-up image from the LCOGT 1-m network (bottom-right). All images are on the same angular scale and the position of ASASSN-15lh is marked.
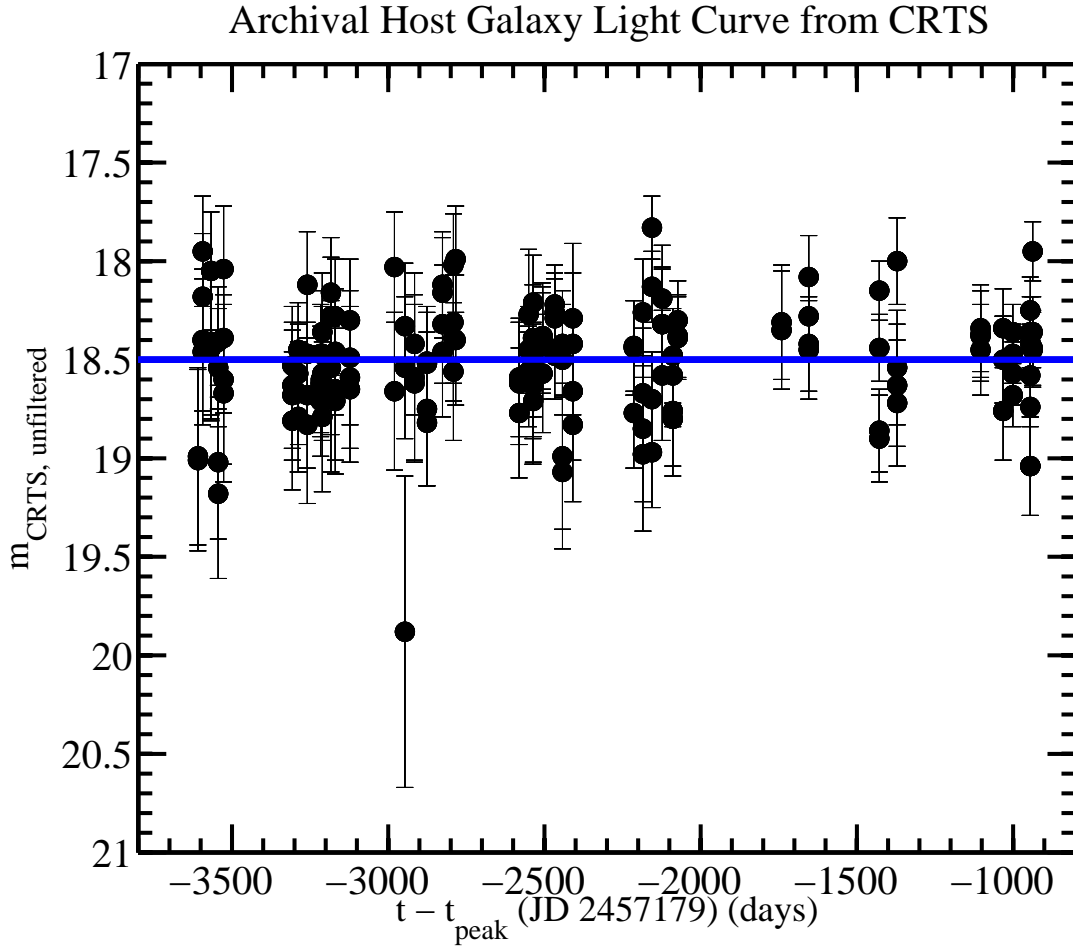
**Figure S2.** Pre-explosion archival un-filtered photometry of APMUKS(BJ) B215839.70-615403.9 (host galaxy of ASASSN-15lh) from the CRTS survey. The axis shows the time of observation with respect to the peak date of ASASSN-15lh. The mean magnitude is $18.5$ (blue line). Over $\sim 7.3$ years of monitoring, the host is consistent with no photometric variability at the level of $0.3\,\mathrm{mag}$.
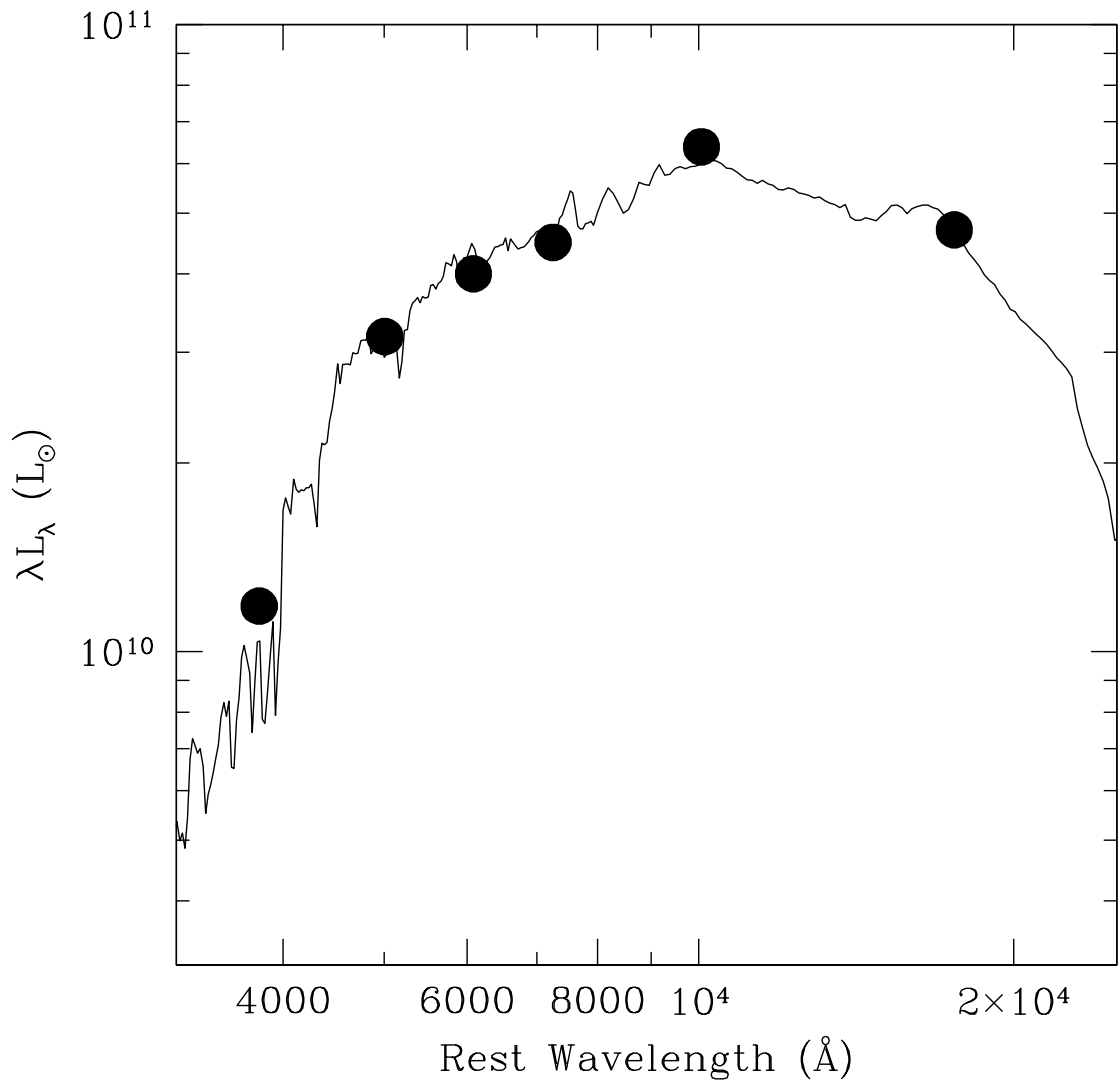
**Figure S3.** SED of APMUKS(BJ) B215839.70-615403.9 (host galaxy of ASASSN-15lh) from pre-explosion archival data is shown in solid dots. The best-fit galaxy spectrum is shown as a thin solid line. See Supplementary text for details.
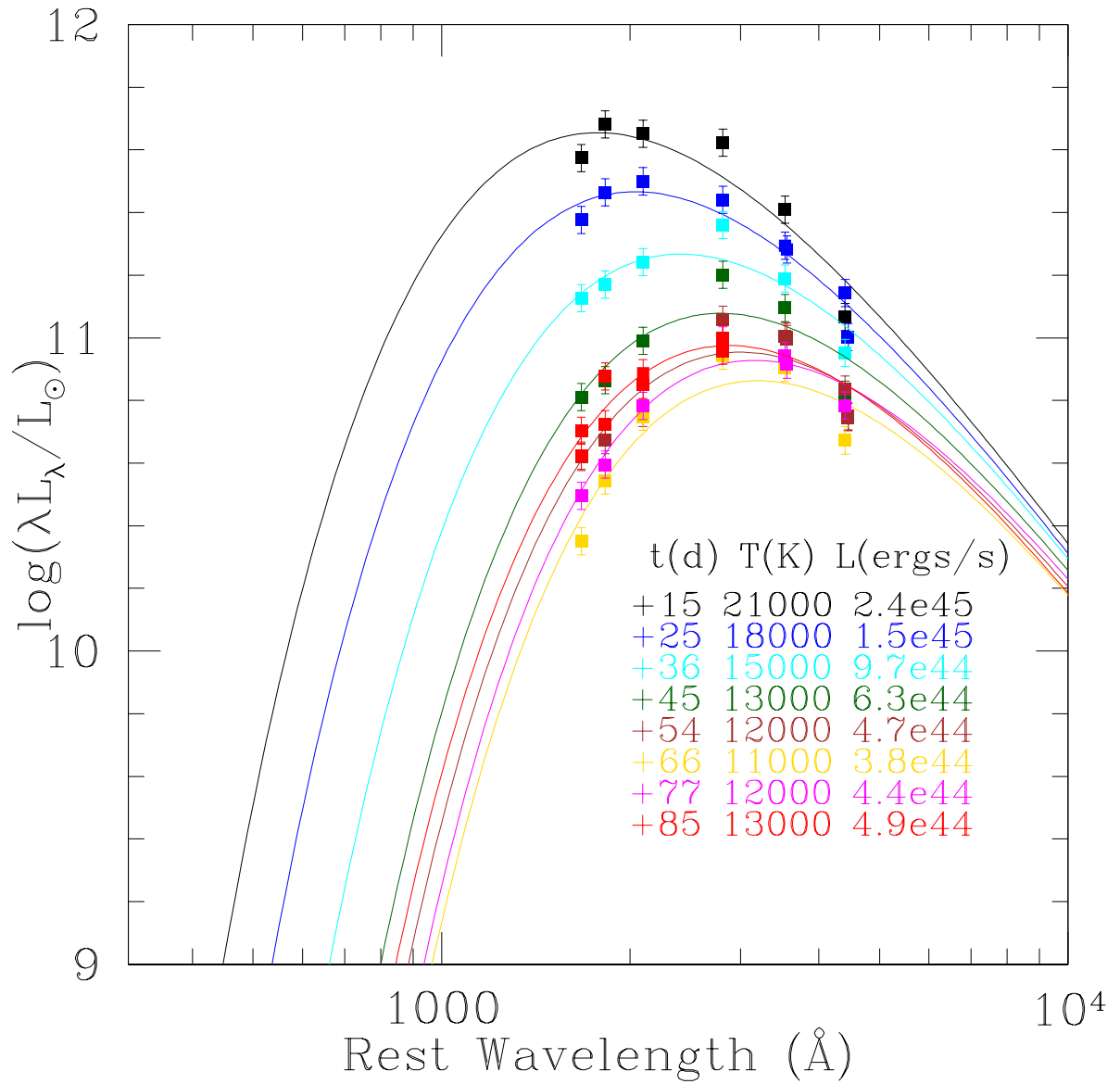
**Figure S4.** The evolution of the SED of ASASSN-15lh. Filled circles with error bars show the observed SED and the best-fit blackbody models are shown in solid lines. The best-fit temperatures and luminosities are listed at the corresponding phases.
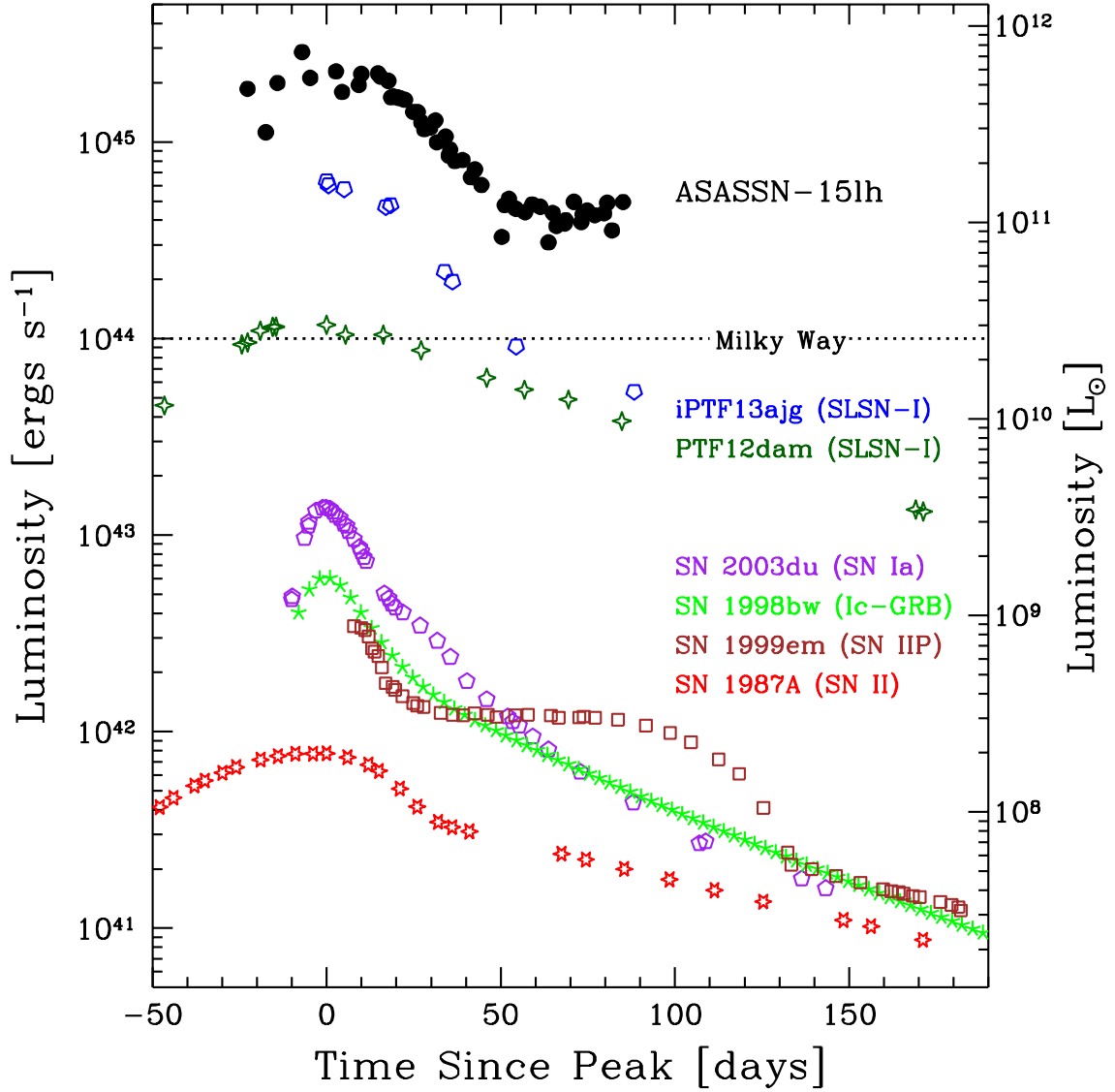
**Figure S5.** Bolometric light curves of ASASSN-15lh and other supernovae for comparison. The bolometric light curves of hydrogen-poor supernovae iPTFajg, PTF12dam, Type Ia supernova SN 2003du, Type Ic-GRB ("hypernova") SN 1998bw, Type IIP supernova SN 1999em and Type II supernova SN 1987A are plotted. The bolometric luminosity of the Milky Way galaxy is shown as a dashed line.

17

Table S1: The Five Most Luminous SNe

| Name | $L_{\mathrm{peak}}$ $(\mathrm{ergs\,s^{-1}})$ | Type | Ref. |
|------|------|------|------|
| ASASSN-15lh | $2.2 \times 10^{45}$ | SLSN-I | This Work |
| CSS100217 | $1.3 \times 10^{45}$ | SLSN-II? | (*55*) |
| CSS121015 | $8.5 \times 10^{44}$ | SLSN-II | (*64*) |
| SN 2008es | $6.3 \times 10^{44}$ | SLSN-II | (*65*) |
| iPTF13ajg | $6.3 \times 10^{44}$ | SLSN-I | (*17*) |

We list the peak luminosities and types of the five most luminous SNe discovered to date. ASASSN-15lh is $\gtrsim 2$ times more luminous than any other SN. Note that CSS100217 is found at the core of an AGN, and whether it is a TDE, AGN transient, or an SLSN-II is debated (see Supplementary text).

Table S2: Blackbody Temperature $T_{\mathrm{BB}}$, Radius $R_{\mathrm{BB}}$ and bolometric luminosity L derived from SED fitting with a linear temperature prior at early time.

| MJD | $N_{\mathrm{obs}}$ | $\log L(L_\odot)$ | $\log L_-$ | $\log L_+$ | $\log T(K)$ | $\log T_-$ | $\log T_+$ | $\log R(cm)$ | $\log R_-$ | $\log R_+$ |
|---|---|---|---|---|---|---|---|---|---|---|
| 57150.5 | 1 | 11.69 | 11.49 | 11.89 | 4.44 | 4.36 | 4.52 | 15.34 | 15.26 | 15.42 |
| 57157.0 | 1 | 11.46 | 11.28 | 11.67 | 4.41 | 4.33 | 4.50 | 15.28 | 15.20 | 15.36 |
| 57161.1 | 1 | 11.72 | 11.53 | 11.91 | 4.40 | 4.32 | 4.49 | 15.42 | 15.34 | 15.50 |
| 57169.8 | 1 | 11.87 | 11.69 | 12.07 | 4.38 | 4.30 | 4.46 | 15.55 | 15.46 | 15.63 |
| 57172.7 | 1 | 11.74 | 11.56 | 11.94 | 4.37 | 4.28 | 4.45 | 15.51 | 15.42 | 15.59 |
| 57181.8 | 1 | 11.78 | 11.60 | 11.97 | 4.33 | 4.25 | 4.42 | 15.59 | 15.51 | 15.68 |
| 57184.0 | 1 | 11.67 | 11.50 | 11.86 | 4.32 | 4.24 | 4.41 | 15.56 | 15.47 | 15.65 |
| 57189.9 | 2 | 11.71 | 11.55 | 11.88 | 4.30 | 4.22 | 4.38 | 15.62 | 15.53 | 15.71 |
| 57190.8 | 4 | 11.76 | 11.61 | 11.92 | 4.35 | 4.28 | 4.42 | 15.55 | 15.48 | 15.63 |
| 57196.7 | 4 | 11.76 | 11.63 | 11.91 | 4.31 | 4.24 | 4.38 | 15.63 | 15.55 | 15.72 |
| 57197.5 | 6 | 11.75 | 11.71 | 11.79 | 4.29 | 4.26 | 4.33 | 15.66 | 15.60 | 15.71 |
| 57200.3 | 7 | 11.73 | 11.69 | 11.78 | 4.32 | 4.29 | 4.35 | 15.60 | 15.55 | 15.65 |
| 57201.3 | 3 | 11.64 | 11.51 | 11.80 | 4.31 | 4.24 | 4.38 | 15.57 | 15.49 | 15.65 |
| 57202.2 | 6 | 11.65 | 11.62 | 11.68 | 4.23 | 4.20 | 4.26 | 15.73 | 15.67 | 15.79 |
| 57203.6 | 2 | 11.64 | 11.51 | 11.79 | 4.28 | 4.20 | 4.35 | 15.64 | 15.55 | 15.73 |
| 57204.7 | 2 | 11.64 | 11.51 | 11.78 | 4.27 | 4.20 | 4.35 | 15.64 | 15.55 | 15.74 |
| 57206.2 | 8 | 11.63 | 11.60 | 11.66 | 4.26 | 4.23 | 4.29 | 15.67 | 15.62 | 15.72 |
| 57209.1 | 8 | 11.57 | 11.54 | 11.60 | 4.23 | 4.21 | 4.26 | 15.69 | 15.64 | 15.74 |
| 57210.7 | 1 | 11.57 | 11.45 | 11.71 | 4.22 | 4.13 | 4.30 | 15.72 | 15.61 | 15.85 |
| 57212.0 | 6 | 11.52 | 11.49 | 11.55 | 4.20 | 4.17 | 4.22 | 15.73 | 15.68 | 15.79 |
| 57213.0 | 2 | 11.48 | 11.37 | 11.61 | 4.22 | 4.15 | 4.30 | 15.66 | 15.57 | 15.76 |
| 57215.2 | 6 | 11.49 | 11.46 | 11.52 | 4.20 | 4.17 | 4.23 | 15.71 | 15.65 | 15.77 |
| 57217.0 | 2 | 11.53 | 11.46 | 11.60 | 4.13 | 4.09 | 4.17 | 15.88 | 15.78 | 15.98 |
| 57217.5 | 3 | 11.41 | 11.37 | 11.46 | 4.20 | 4.17 | 4.24 | 15.67 | 15.61 | 15.72 |
| 57220.6 | 4 | 11.44 | 11.39 | 11.50 | 4.13 | 4.10 | 4.16 | 15.83 | 15.74 | 15.92 |
| 57221.7 | 2 | 11.35 | 11.24 | 11.47 | 4.19 | 4.12 | 4.27 | 15.65 | 15.56 | 15.76 |
| 57222.2 | 6 | 11.38 | 11.35 | 11.41 | 4.17 | 4.14 | 4.19 | 15.72 | 15.67 | 15.78 |
| 57223.9 | 7 | 11.32 | 11.29 | 11.35 | 4.17 | 4.14 | 4.19 | 15.70 | 15.65 | 15.74 |
| 57226.6 | 6 | 11.32 | 11.29 | 11.36 | 4.11 | 4.09 | 4.14 | 15.80 | 15.75 | 15.86 |
| 57229.6 | 7 | 11.24 | 11.21 | 11.27 | 4.12 | 4.10 | 4.15 | 15.74 | 15.69 | 15.79 |
| 57231.0 | 1 | 11.28 | 11.19 | 11.37 | 4.11 | 4.03 | 4.19 | 15.79 | 15.66 | 15.94 |
| 57233.3 | 6 | 11.20 | 11.16 | 11.23 | 4.10 | 4.08 | 4.13 | 15.76 | 15.71 | 15.81 |
| 57240.5 | 1 | 10.93 | 10.84 | 11.04 | 4.04 | 3.96 | 4.13 | 15.74 | 15.62 | 15.88 |
| 57241.5 | 7 | 11.09 | 11.06 | 11.12 | 4.09 | 4.07 | 4.11 | 15.73 | 15.69 | 15.78 |
| 57243.0 | 2 | 11.13 | 11.05 | 11.22 | 4.10 | 4.03 | 4.17 | 15.74 | 15.63 | 15.85 |
| 57245.4 | 10 | 11.08 | 11.05 | 11.10 | 4.07 | 4.06 | 4.09 | 15.76 | 15.72 | 15.80 |
| 57248.7 | 7 | 11.06 | 11.03 | 11.09 | 4.07 | 4.05 | 4.09 | 15.76 | 15.72 | 15.81 |
| 57251.2 | 8 | 11.10 | 11.07 | 11.13 | 4.06 | 4.04 | 4.08 | 15.80 | 15.76 | 15.84 |
| 57254.1 | 7 | 11.09 | 11.05 | 11.12 | 4.06 | 4.05 | 4.08 | 15.79 | 15.74 | 15.83 |
| 57257.0 | 1 | 10.90 | 10.81 | 11.01 | 4.04 | 3.96 | 4.12 | 15.74 | 15.62 | 15.88 |
| 57258.5 | 2 | 11.05 | 10.98 | 11.15 | 4.11 | 4.04 | 4.18 | 15.68 | 15.58 | 15.80 |
| 57259.8 | 6 | 10.99 | 10.95 | 11.03 | 4.05 | 4.03 | 4.07 | 15.77 | 15.72 | 15.82 |

Table S2 cont.

| MJD | $N_{\mathrm{obs}}$ | $\log L(L_\odot)$ | $\log L_-$ | $\log L_+$ | $\log T(K)$ | $\log T_-$ | $\log T_+$ | $\log R(cm)$ | $\log R_-$ | $\log R_+$ |
|---|---|---|---|---|---|---|---|---|---|---|
| 57261.6 | 2 | 11.01 | 10.93 | 11.10 | 4.11 | 4.04 | 4.18 | 15.65 | 15.55 | 15.77 |
| 57262.8 | 2 | 11.00 | 10.93 | 11.08 | 4.07 | 4.00 | 4.14 | 15.72 | 15.61 | 15.85 |
| 57263.1 | 8 | 11.02 | 10.99 | 11.05 | 4.05 | 4.03 | 4.07 | 15.78 | 15.74 | 15.82 |
| 57266.0 | 4 | 11.11 | 11.05 | 11.17 | 3.98 | 3.96 | 4.00 | 15.96 | 15.89 | 16.02 |
| 57268.6 | 2 | 11.01 | 10.94 | 11.10 | 4.10 | 4.03 | 4.17 | 15.67 | 15.56 | 15.78 |
| 57269.1 | 6 | 11.05 | 11.01 | 11.09 | 4.03 | 4.01 | 4.05 | 15.84 | 15.79 | 15.89 |
| 57270.7 | 1 | 11.07 | 10.99 | 11.14 | 4.04 | 3.96 | 4.12 | 15.81 | 15.67 | 15.98 |
| 57273.4 | 7 | 11.04 | 11.01 | 11.08 | 4.05 | 4.04 | 4.07 | 15.78 | 15.74 | 15.83 |
| 57276.7 | 1 | 11.05 | 10.98 | 11.13 | 4.04 | 3.96 | 4.12 | 15.81 | 15.66 | 15.98 |
| 57277.8 | 6 | 11.11 | 11.07 | 11.14 | 4.08 | 4.06 | 4.10 | 15.77 | 15.71 | 15.82 |
| 57279.5 | 2 | 10.97 | 10.89 | 11.05 | 4.10 | 4.03 | 4.17 | 15.66 | 15.55 | 15.77 |
| 57283.4 | 8 | 11.11 | 11.06 | 11.16 | 4.08 | 4.06 | 4.11 | 15.76 | 15.68 | 15.83 |

Table S3: Blackbody Temperature $T_{\mathrm{BB}}$, Radius $R_{\mathrm{BB}}$ and bolometric luminosity L derived from SED fitting with a flat temperature prior at early time.

| MJD | $N_{\mathrm{obs}}$ | $\log L(L_\odot)$ | $\log L_-$ | $\log L_+$ | $\log T(K)$ | $\log T_-$ | $\log T_+$ | $\log R(cm)$ | $\log R_-$ | $\log R_+$ |
|---|---|---|---|---|---|---|---|---|---|---|
| 57150.5 | 1 | 11.39 | 11.22 | 11.58 | 4.30 | 4.22 | 4.38 | 15.47 | 15.38 | 15.56 |
| 57157.0 | 1 | 11.22 | 11.06 | 11.40 | 4.30 | 4.22 | 4.38 | 15.38 | 15.30 | 15.48 |
| 57161.1 | 1 | 11.49 | 11.33 | 11.67 | 4.30 | 4.22 | 4.38 | 15.52 | 15.43 | 15.61 |
| 57169.8 | 1 | 11.71 | 11.54 | 11.89 | 4.30 | 4.22 | 4.38 | 15.62 | 15.54 | 15.72 |
| 57172.7 | 1 | 11.60 | 11.43 | 11.78 | 4.30 | 4.22 | 4.38 | 15.57 | 15.48 | 15.67 |
| 57181.8 | 1 | 11.71 | 11.53 | 11.90 | 4.30 | 4.22 | 4.38 | 15.62 | 15.54 | 15.72 |
| 57184.0 | 1 | 11.62 | 11.45 | 11.80 | 4.30 | 4.21 | 4.38 | 15.58 | 15.49 | 15.68 |
| 57189.9 | 2 | 11.70 | 11.54 | 11.87 | 4.30 | 4.22 | 4.38 | 15.62 | 15.54 | 15.71 |
| 57190.8 | 4 | 11.76 | 11.61 | 11.92 | 4.35 | 4.28 | 4.42 | 15.55 | 15.48 | 15.63 |
| 57196.7 | 4 | 11.76 | 11.63 | 11.91 | 4.31 | 4.24 | 4.38 | 15.63 | 15.55 | 15.72 |
| 57197.5 | 6 | 11.75 | 11.71 | 11.79 | 4.29 | 4.26 | 4.33 | 15.66 | 15.60 | 15.71 |
| 57200.3 | 7 | 11.73 | 11.68 | 11.77 | 4.32 | 4.29 | 4.35 | 15.60 | 15.55 | 15.65 |
| 57201.3 | 3 | 11.65 | 11.51 | 11.80 | 4.31 | 4.24 | 4.38 | 15.57 | 15.49 | 15.66 |
| 57202.2 | 6 | 11.65 | 11.62 | 11.68 | 4.23 | 4.20 | 4.26 | 15.73 | 15.67 | 15.79 |
| 57203.6 | 2 | 11.64 | 11.51 | 11.78 | 4.28 | 4.20 | 4.35 | 15.64 | 15.56 | 15.73 |
| 57204.7 | 2 | 11.63 | 11.51 | 11.78 | 4.27 | 4.20 | 4.35 | 15.64 | 15.56 | 15.74 |
| 57206.2 | 8 | 11.63 | 11.60 | 11.66 | 4.26 | 4.23 | 4.29 | 15.67 | 15.62 | 15.72 |
| 57209.1 | 8 | 11.57 | 11.54 | 11.60 | 4.23 | 4.21 | 4.26 | 15.69 | 15.64 | 15.74 |
| 57210.7 | 1 | 11.57 | 11.45 | 11.71 | 4.22 | 4.14 | 4.30 | 15.72 | 15.61 | 15.84 |
| 57212.0 | 6 | 11.52 | 11.49 | 11.55 | 4.20 | 4.17 | 4.22 | 15.73 | 15.68 | 15.79 |
| 57213.0 | 2 | 11.48 | 11.37 | 11.62 | 4.23 | 4.15 | 4.30 | 15.66 | 15.57 | 15.76 |
| 57215.2 | 6 | 11.49 | 11.46 | 11.52 | 4.20 | 4.18 | 4.23 | 15.71 | 15.65 | 15.77 |
| 57217.0 | 2 | 11.53 | 11.46 | 11.59 | 4.13 | 4.09 | 4.17 | 15.88 | 15.78 | 15.97 |
| 57217.5 | 3 | 11.41 | 11.37 | 11.46 | 4.21 | 4.17 | 4.24 | 15.67 | 15.61 | 15.72 |
| 57220.6 | 4 | 11.44 | 11.38 | 11.50 | 4.13 | 4.10 | 4.17 | 15.83 | 15.74 | 15.92 |
| 57221.7 | 2 | 11.35 | 11.24 | 11.47 | 4.20 | 4.12 | 4.27 | 15.65 | 15.56 | 15.76 |
| 57222.2 | 6 | 11.38 | 11.35 | 11.41 | 4.17 | 4.14 | 4.19 | 15.73 | 15.67 | 15.78 |
| 57223.9 | 7 | 11.32 | 11.29 | 11.35 | 4.17 | 4.14 | 4.19 | 15.70 | 15.65 | 15.74 |
| 57226.6 | 6 | 11.32 | 11.29 | 11.36 | 4.11 | 4.09 | 4.14 | 15.80 | 15.75 | 15.86 |
| 57229.6 | 7 | 11.24 | 11.21 | 11.27 | 4.12 | 4.10 | 4.15 | 15.74 | 15.69 | 15.79 |
| 57231.0 | 1 | 11.28 | 11.19 | 11.38 | 4.11 | 4.03 | 4.19 | 15.79 | 15.66 | 15.94 |
| 57233.3 | 6 | 11.20 | 11.16 | 11.23 | 4.10 | 4.08 | 4.13 | 15.76 | 15.71 | 15.81 |
| 57240.5 | 1 | 10.93 | 10.84 | 11.05 | 4.05 | 3.96 | 4.13 | 15.74 | 15.62 | 15.88 |
| 57241.5 | 7 | 11.09 | 11.06 | 11.12 | 4.09 | 4.07 | 4.11 | 15.73 | 15.69 | 15.78 |
| 57243.0 | 2 | 11.12 | 11.05 | 11.21 | 4.10 | 4.03 | 4.17 | 15.74 | 15.63 | 15.85 |
| 57245.4 | 10 | 11.08 | 11.05 | 11.10 | 4.07 | 4.06 | 4.09 | 15.76 | 15.72 | 15.80 |
| 57248.7 | 7 | 11.06 | 11.03 | 11.09 | 4.07 | 4.05 | 4.09 | 15.76 | 15.72 | 15.81 |
| 57251.2 | 8 | 11.10 | 11.07 | 11.13 | 4.06 | 4.04 | 4.08 | 15.80 | 15.76 | 15.84 |
| 57254.1 | 7 | 11.09 | 11.05 | 11.12 | 4.06 | 4.05 | 4.08 | 15.79 | 15.74 | 15.83 |
| 57257.0 | 1 | 10.90 | 10.81 | 11.02 | 4.04 | 3.96 | 4.12 | 15.74 | 15.62 | 15.88 |
| 57258.5 | 2 | 11.06 | 10.98 | 11.15 | 4.11 | 4.04 | 4.18 | 15.68 | 15.58 | 15.79 |
| 57259.8 | 6 | 10.99 | 10.95 | 11.03 | 4.05 | 4.03 | 4.07 | 15.77 | 15.72 | 15.82 |

Table S3 cont.

| MJD | $N_{\mathrm{obs}}$ | $\log L(L_\odot)$ | $\log L_-$ | $\log L_+$ | $\log T(K)$ | $\log T_-$ | $\log T_+$ | $\log R(cm)$ | $\log R_-$ | $\log R_+$ |
|---|---|---|---|---|---|---|---|---|---|---|
| 57261.6 | 2 | 11.01 | 10.93 | 11.10 | 4.11 | 4.04 | 4.18 | 15.66 | 15.55 | 15.77 |
| 57262.8 | 2 | 11.00 | 10.94 | 11.08 | 4.07 | 4.00 | 4.14 | 15.72 | 15.61 | 15.85 |
| 57263.1 | 8 | 11.02 | 10.99 | 11.05 | 4.05 | 4.03 | 4.07 | 15.78 | 15.74 | 15.82 |
| 57266.0 | 4 | 11.11 | 11.05 | 11.17 | 3.98 | 3.96 | 4.00 | 15.96 | 15.89 | 16.03 |
| 57268.6 | 2 | 11.01 | 10.93 | 11.10 | 4.10 | 4.03 | 4.17 | 15.67 | 15.56 | 15.79 |
| 57269.1 | 6 | 11.05 | 11.01 | 11.09 | 4.03 | 4.01 | 4.05 | 15.84 | 15.79 | 15.89 |
| 57270.7 | 1 | 11.07 | 10.99 | 11.14 | 4.04 | 3.96 | 4.12 | 15.81 | 15.67 | 15.99 |
| 57273.4 | 7 | 11.04 | 11.01 | 11.08 | 4.05 | 4.04 | 4.07 | 15.78 | 15.73 | 15.83 |
| 57276.7 | 1 | 11.05 | 10.98 | 11.13 | 4.04 | 3.96 | 4.12 | 15.81 | 15.66 | 15.97 |
| 57277.8 | 6 | 11.11 | 11.07 | 11.14 | 4.08 | 4.06 | 4.10 | 15.77 | 15.71 | 15.82 |
| 57279.5 | 2 | 10.97 | 10.89 | 11.05 | 4.10 | 4.03 | 4.17 | 15.66 | 15.55 | 15.77 |
| 57283.4 | 8 | 11.11 | 11.06 | 11.16 | 4.08 | 4.06 | 4.11 | 15.76 | 15.68 | 15.83 |

Table S4: ASAS-SN $V$-band photometry with image subtraction

| MJD | $V$ | $e_V$ |
|---|---|---|
| 57110.69520 | > 17.64 | - |
| 57118.39377 | > 17.52 | - |
| 57124.75369 | > 17.62 | - |
| 57127.05225 | > 17.82 | - |
| 57136.35575 | > 17.79 | - |
| 57136.88918 | > 18.30 | - |
| 57150.03689 | 17.39 | 0.23 |
| 57156.55688 | 17.64 | 0.19 |
| 57160.65807 | 17.22 | 0.14 |
| 57169.34084 | 16.83 | 0.14 |
| 57172.30403 | 17.03 | 0.18 |
| 57181.35200 | 16.82 | 0.13 |
| 57183.50502 | 16.99 | 0.13 |
| 57190.21255 | 17.24 | 0.16 |
| 57190.29006 | 16.94 | 0.10 |
| 57200.23218 | 17.38 | 0.19 |
| 57200.71115 | 17.28 | 0.24 |

Table S5: *Swift* UVOT Photometry

*Swift* UVOT Aperture photometry (Johnson-Kron/Cousins) with no host subtraction.

| MJD | $UW2$ | $e_{UW2}$ | $UM2$ | $e_{UM2}$ | $UW1$ | $e_{UW1}$ | $U$ | $e_U$ | $B$ | $e_B$ | $V$ | $e_V$ |
|---|---|---|---|---|---|---|---|---|---|---|---|---|
| 57197.03 | 15.59 | 0.05 | 15.24 | 0.06 | 15.29 | 0.05 | 15.39 | 0.04 | 16.76 | 0.06 | 17.07 | 0.14 |
| 57199.76 | 15.69 | 0.05 | 15.32 | 0.05 | 15.31 | 0.05 | 15.45 | 0.04 | 16.75 | 0.05 | 16.77 | 0.10 |
| 57201.75 | 15.97 | 0.05 | 15.58 | 0.06 | 15.41 | 0.05 | 15.52 | 0.05 | 16.89 | 0.06 | 16.96 | 0.13 |
| 57205.53 | 15.90 | 0.05 | 15.61 | 0.05 | 15.56 | 0.05 | 15.60 | 0.05 | 16.96 | 0.06 | 16.92 | 0.11 |
| 57208.60 | 16.09 | 0.07 | 15.78 | 0.06 | 15.68 | 0.07 | 15.83 | 0.07 | 17.02 | 0.09 | 16.87 | 0.17 |
| 57211.52 | 16.34 | 0.07 | 15.96 | 0.06 | 15.90 | 0.07 | 15.75 | 0.07 | 17.10 | 0.09 | 17.09 | 0.17 |
| 57214.68 | 16.35 | 0.04 | 16.09 | 0.05 | 15.94 | 0.04 | 15.87 | 0.04 | 17.09 | 0.05 | 17.20 | 0.10 |
| 57216.50 | 16.55 | 0.09 | - | - | - | - | 15.90 | 0.03 | - | - | - | - |
| 57217.38 | 16.43 | 0.04 | - | - | - | - | - | - | - | - | - | - |
| 57219.69 | 16.61 | 0.10 | - | - | 16.27 | 0.06 | - | - | - | - | - | - |
| 57220.50 | 16.77 | 0.09 | - | - | - | - | 16.09 | 0.04 | - | - | - | - |
| 57221.68 | 16.71 | 0.06 | 16.52 | 0.06 | 16.31 | 0.06 | 16.03 | 0.05 | 17.29 | 0.07 | 17.31 | 0.13 |
| 57223.48 | 16.87 | 0.06 | 16.69 | 0.06 | 16.41 | 0.06 | 16.17 | 0.06 | 17.36 | 0.07 | 17.26 | 0.13 |
| 57226.09 | 17.14 | 0.09 | 16.81 | 0.10 | 16.56 | 0.09 | 16.28 | 0.07 | 17.39 | 0.09 | 17.14 | 0.15 |
| 57229.14 | 17.38 | 0.11 | 16.92 | 0.10 | 16.67 | 0.10 | 16.62 | 0.12 | 17.34 | 0.12 | 17.53 | 0.26 |
| 57232.80 | 17.48 | 0.09 | 17.27 | 0.09 | 16.94 | 0.09 | 16.42 | 0.08 | 17.50 | 0.10 | 17.55 | 0.20 |
| 57241.06 | 17.84 | 0.09 | 17.58 | 0.08 | 17.23 | 0.08 | 16.67 | 0.07 | 17.56 | 0.08 | 17.67 | 0.16 |
| 57244.85 | 17.94 | 0.10 | 17.73 | 0.09 | 17.50 | 0.10 | 16.77 | 0.08 | 17.72 | 0.09 | 17.52 | 0.16 |
| 57248.37 | 18.10 | 0.10 | 17.77 | 0.10 | 17.47 | 0.10 | 16.77 | 0.09 | 17.60 | 0.10 | 17.68 | 0.20 |
| 57250.71 | 18.07 | 0.10 | 17.81 | 0.10 | 17.31 | 0.10 | 16.83 | 0.09 | 17.50 | 0.09 | 17.36 | 0.16 |
| 57253.62 | 18.10 | 0.13 | 17.77 | 0.12 | 17.37 | 0.13 | 16.63 | 0.10 | 17.69 | 0.12 | 17.39 | 0.21 |
| 57259.27 | 18.57 | 0.16 | 18.04 | 0.13 | 17.53 | 0.13 | 17.05 | 0.12 | 17.95 | 0.14 | 17.80 | 0.27 |
| 57262.59 | 18.34 | 0.16 | 18.11 | 0.14 | 17.47 | 0.13 | 17.03 | 0.13 | 17.82 | 0.14 | 17.59 | 0.25 |
| 57265.53 | 18.91 | 0.33 | - | - | 17.52 | 0.10 | 17.00 | 0.09 | 17.97 | 0.11 | - | - |
| 57268.65 | 18.45 | 0.12 | 18.06 | 0.10 | 17.62 | 0.10 | 17.02 | 0.09 | 17.83 | 0.10 | 17.58 | 0.17 |
| 57272.84 | 18.14 | 0.10 | 17.98 | 0.16 | 17.53 | 0.10 | 16.99 | 0.09 | 17.84 | 0.11 | 17.64 | 0.19 |
| 57277.29 | 17.84 | 0.08 | 17.67 | 0.10 | 17.15 | 0.08 | 16.89 | 0.06 | 17.74 | 0.07 | 17.53 | 0.11 |
| 57282.81 | 17.75 | 0.10 | 17.61 | 0.13 | 17.19 | 0.10 | 16.91 | 0.09 | - | - | - | - |
| 57283.07 | 17.94 | 0.10 | 17.24 | 0.11 | 17.27 | 0.10 | 17.02 | 0.09 | - | - | - | - |
| 57284.21 | 17.75 | 0.10 | 17.36 | 0.09 | 17.18 | 0.10 | 16.98 | 0.10 | 17.85 | 0.12 | 17.95 | 0.25 |

Table S6: LCOGT Photometry

LCOGT DoPHOT photometry (Johnson-Kron/Cousins) with no host subtraction.

| MJD | $B$ | $e_B$ | $V$ | $e_V$ |
|---|---|---|---|---|
| 57189.444 | - | - | 16.91 | 0.03 |
| 57190.421 | 16.74 | 0.07 | 16.92 | 0.05 |
| 57196.164 | 16.79 | 0.04 | 16.92 | 0.03 |
| 57200.804 | 16.86 | 0.06 | 17.00 | 0.04 |
| 57203.138 | 16.90 | 0.06 | 17.06 | 0.04 |
| 57204.193 | 16.91 | 0.06 | 17.06 | 0.04 |
| 57206.194 | 16.95 | 0.06 | 17.13 | 0.05 |
| 57208.625 | 17.04 | 0.05 | 17.15 | 0.03 |
| 57210.260 | 17.03 | 0.06 | - | - |
| 57212.524 | 17.15 | 0.06 | 17.16 | 0.04 |
| 57216.869 | 17.18 | 0.07 | 17.27 | 0.07 |
| 57221.188 | 17.33 | 0.06 | 17.36 | 0.04 |
| 57222.884 | - | - | 17.43 | 0.05 |
| 57228.724 | 17.52 | 0.08 | - | - |
| 57230.505 | 17.46 | 0.09 | - | - |
| 57240.034 | - | - | 17.65 | 0.04 |
| 57241.011 | - | - | 17.60 | 0.04 |
| 57242.508 | 17.62 | 0.06 | 17.53 | 0.04 |
| 57244.977 | 17.70 | 0.04 | 17.62 | 0.03 |
| 57247.544 | - | - | 17.61 | 0.04 |
| 57250.526 | 17.78 | 0.07 | 17.71 | 0.04 |
| 57253.515 | - | - | 17.72 | 0.04 |
| 57256.599 | - | - | 17.69 | 0.06 |
| 57258.035 | 17.75 | 0.09 | 17.70 | 0.07 |
| 57261.087 | 17.86 | 0.07 | 17.79 | 0.06 |
| 57262.287 | 17.95 | 0.11 | 17.64 | 0.10 |
| 57262.616 | 17.79 | 0.07 | 17.77 | 0.07 |
| 57268.141 | 17.87 | 0.05 | 17.75 | 0.03 |
| 57270.208 | 17.88 | 0.05 | - | - |
| 57273.206 | 17.89 | 0.05 | - | - |
| 57276.279 | 17.91 | 0.05 | - | - |
| 57279.015 | 17.98 | 0.08 | 17.80 | 0.05 |